Bioconjugate Chemistry

Article

pubs.acs.org/bc

Magnetic Prussian Blue Nanoparticles for Targeted Photothermal Therapy under Magnetic Resonance Imaging Guidance

Guanglei Fu,[‡] Wei Liu,[‡] Yanyan Li,[‡] Yushen Jin,[‡] Lingdong Jiang,[‡] Xiaolong Liang,[†] Shanshan Feng,[‡] and Zhifei Dai*[,†]

[†]Department of Biomedical Engineering, College of Engineering, Peking University, Beijing 100871, P.R. China

[‡]Nanomedicine and Biosensor Laboratory, School of Life Science and Technology, Harbin Institute of Technology, Harbin 150001, P.R. China

Supporting Information

ABSTRACT: This paper reported a core−shell nanotheranostic agent by growing Prussian blue (PB) nanoshells of 3−6 nm around superparamagnetic Fe_3O_4 nanocores for targeted photothermal therapy of cancer under magnetic resonance imaging (MRI) guidance. Both *in vitro* and *in vivo* experiments proved that the Fe_3O_4@PB core−shell nanoparticles showed significant contrast enhancement for T_2-weighted MRI with the relaxivity value of 58.9 $mM^{-1}\cdot s^{-1}$. Simultaneously, the composite nanoparticles exhibited a high photothermal effect under irradiation of a near-infrared laser due to the strong absorption of PB nanoshells, which led to more than 80% death of HeLa cells with only 0.016 $mg\cdot mL^{-1}$ of the nanoparticles with the aid of the magnetic targeting effect. Using tumor-bearing nude mice as the model, the near-infrared laser light ablated the tumor effectively in the presence of the Fe_3O_4@PB nanoparticles and the tumor growth inhibition was evaluated to be 87.2%. Capabilities of MRI, magnetic targeting, and photothermal therapy were thus integrated into a single agent to allow efficient MRI-guided targeted photothermal therapy. Most importantly, both PB and Fe_3O_4 nanoparticles were already clinically approved drugs, so the Fe_3O_4@PB nanoparticles as a theranostic nanomedicine would be particularly promising for clinical applications in the human body due to the reliable biosafety.

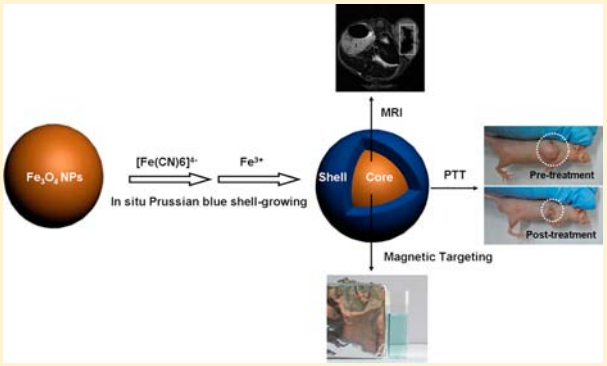

INTRODUCTION

Theranostics has emerged as an attractive treatment strategy for various cancers due to its improved disease prognoses, ease of real-time monitoring of therapy, and more individualized therapies.[1,2] One of the most exciting features of nanoparticles for their use in biomedicine is the capability of easily putting new combinations of different functional molecules into a single nanoparticle.[3,4] The application of multifunctional nanoparticles for biomedical imaging, diagnostics, and therapeutics has enjoyed explosive development to provide a variety of nanoscale platforms for cancer treatment, especially for the theranostic strategy. Nevertheless, up to now, most of the reported theranostic agents are far from clinical application due to their toxicity and complexity of composition and structure. A shortcut to take theranostic agents from bench to bedside should be fabrication of new theranostic agents using U.S. Food and Drug Administration (FDA)-approved materials or imparting advanced theranostic functions to FDA-approved materials.

Multifunctional nanomaterials proposed for image-guided photothermal therapy (PTT) are of particular advantage among various theranostic agents.[4−6] PTT that employs photothermal agents to ablate cancer cells through photothermal conversion has received great research interest as an alternative to classical therapies.[7,8] In combination with PTT, medical imaging shows great promise in identification of tumor locations and assessment of photothermal ablation efficacy to guide PTT.[9,10] Numerous theranostic nanomaterials prepared with a variety of imaging and photothermal components such as carbon-[11−13] and gold-based nanomaterials have been developed.[14−17] However, for their wide applications, these theranostic agents encounter numerous obstacles, such as complicated synthesis procedure, low photothermal stability, and especially potential long-term toxicity.[7] To further improve treatment efficacy and reduce side effects, specified targeting capability of theranostic agents to tumor sites is also challengeable. Hence, the development of theranostic nanomaterials with tumor targeting capability and reliable biosafety in the human body is urgently desired to meet the clinical requirements.

Prussian blue (PB), a prototype of mixed-valence transition metal hexacyanoferrates, is an ancient dye with low cost and simple preparation.[18−20] Due to strong optical absorbance in the near-infrared region (NIR) and high photothermal

Received: June 25, 2014
Revised: August 2, 2014
Published: August 9, 2014

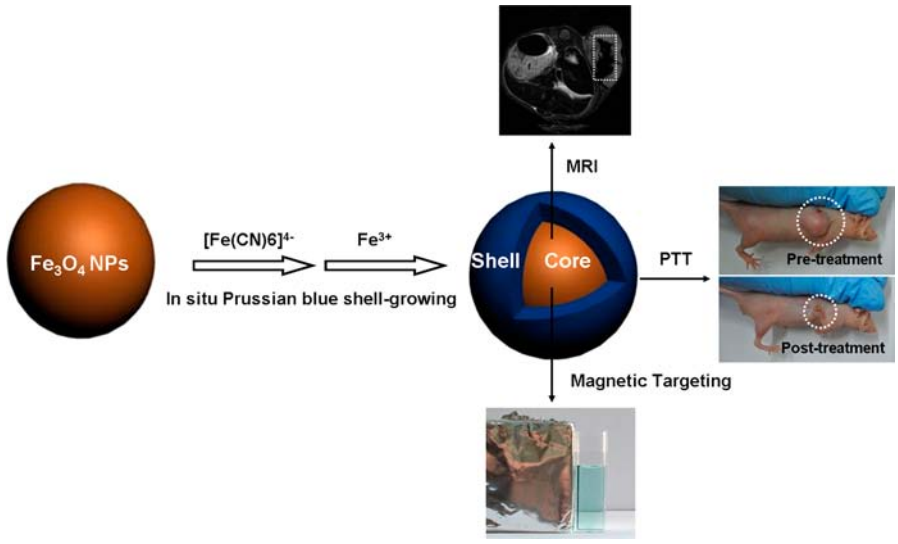

Figure 1. Illustration of the synthesis procedure and theranostic applications of the multifunctional Fe_3O_4@PB NPs.

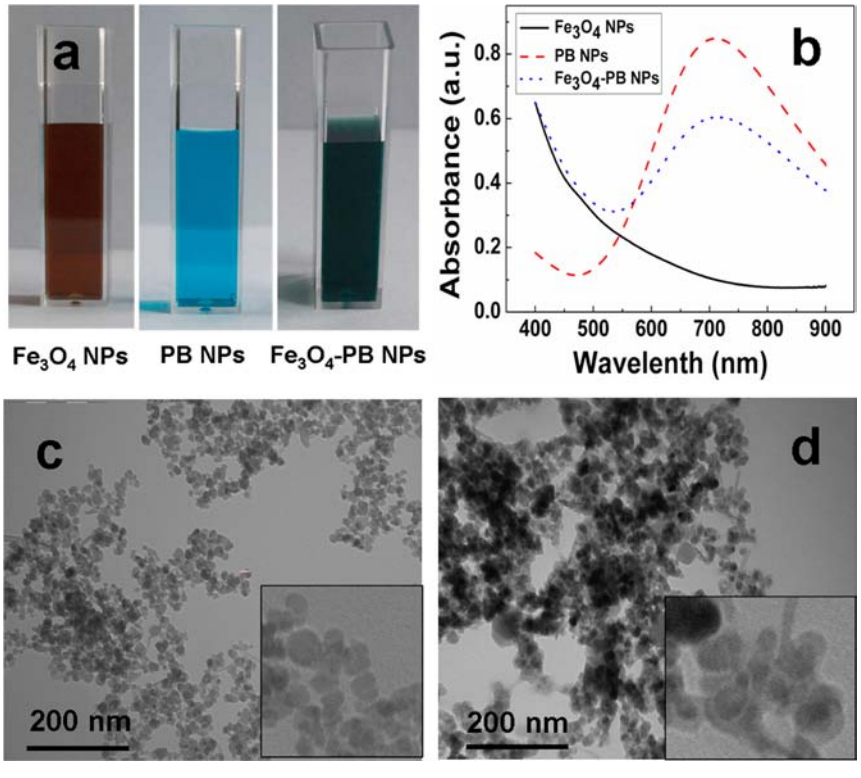

Figure 2. (a) Photographs of aqueous dispersions of the Fe_3O_4 NPs, PB NPs, and Fe_3O_4@PB NPs; (b) UV−vis absorption spectra of the Fe_3O_4 NPs, PB NPs, and Fe_3O_4@PB NPs; (c) TEM images of the Fe_3O_4 NPs; (d) TEM image of the Fe_3O_4@PB NPs.

conversion efficiency, PB-based nanoparticles (NPs) were explored as the new generation of NIR-driven photothermal agent for PTT treatment of cancers.[7−9] On the other hand, magnetic NPs, especially superparamagnetic Fe_3O_4 NPs, have exhibited substantial applications in biomedicine as the contrast enhancement agent for magnetic resonance imaging (MRI)[21−23] as well as for magnetic targeting.[24−26] Most significantly, both Fe_3O_4 NPs and PB have been approved by U.S. FDA for clinical MRI[27,28] and treatment of radioactive exposure[18,29] in the human body, respectively. Thus, the composite nanomaterials formed from Fe_3O_4 NPs and PB would be particularly promising for clinical applications in the human body due to the reliable biosafety.

In this work, we present a Fe_3O_4@PB core−shell nanotheranostic agent with all components from clinically approved drugs for MRI-guided targeted photothermal therapy for cancer. Such multifunctional Fe_3O_4@PB NPs were prepared by forming PB nanoshells around superparamagnetic Fe_3O_4 nanocores through a shell-growing procedure. With the aid of the core−shell composition, capabilities of MRI, magnetic targeting, and photothermal therapy were integrated into a single agent to achieve MRI-guided targeted photothermal therapy. Although the similarly structured NPs have been

dx.doi.org/10.1021/bc500279w | *Bioconjugate Chem.* 2014, 25, 1655−1663

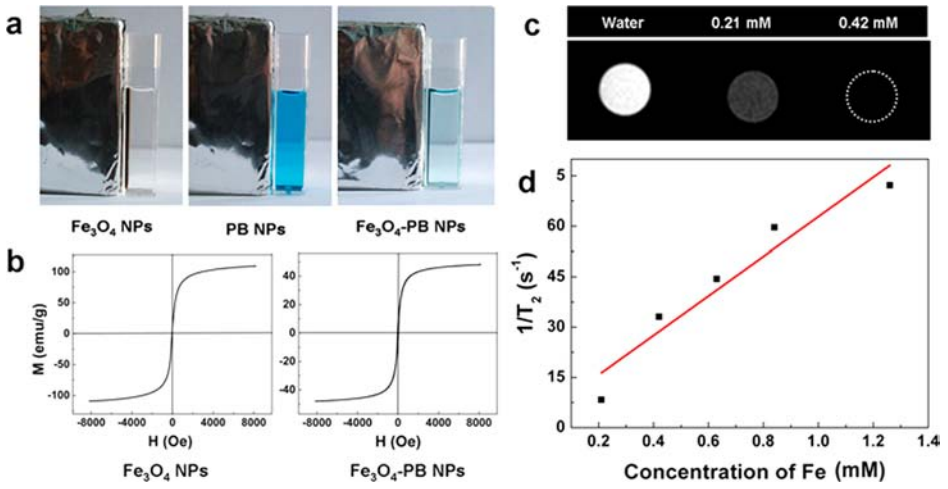

Figure 3. (a) Response of Fe_3O_4 NPs, PB NPs, and Fe_3O_4@PB NPs to a magnetic field. (b) Magnetization curves of Fe_3O_4 NPs and Fe_3O_4@PB NPs at room temperature. (c) T_2-weighted MR images of Fe_3O_4@PB NPs with various iron concentrations. (d) T_2-relaxation rate ($1/T_2$) as a function of iron concentration (mM) in Fe_3O_4@PB NPs.

reported for the peroxidase-like catalytic activity,[19] the finding of the present study is that the Fe_3O_4@PB NPs could operate as a multifunctional nanomedicine for efficient MRI-guided photothermal therapy of cancer.

RESULTS AND DISCUSSION

Preparation and Characterization of Fe_3O_4@PB NPs. The core−shell Fe_3O_4@PB NPs were synthesized by growing PB nanoshells around superparamagnetic Fe_3O_4 nanocores through a shell-growing procedure as illustrated in Figure 1. Aqueous $[Fe(CN)6]^{4-}$ and Fe^{3+} were dropwise added to aqueous dispersions of Fe_3O_4 NPs under acidic condition. The obtained composite Fe_3O_4@PB NPs were then thoroughly purified with magnetic separation to remove the possibly formed pure PB NPs in the suspensions.

After the above shell-growing and magnetic separation procedures, an obvious change from brown to green was observed in the color of the aqueous dispersions as shown in Figure 2a. The color change might be attributed to the color overlap between blue of the possibly formed PB nanoshells and brown of Fe_3O_4 nanocores. Figure 2b shows UV−vis absorption spectra of the NPs before and after the treatment procedures. The as-synthesized Fe_3O_4@PB NPs exhibited a typical absorption peak of PB around 700 nm while Fe_3O_4 NPs showed no absorption peak in this region. The absorption peak was in agreement with that of pure PB NPs due to the charge transfer transition between Fe (II) and Fe (III),[7] indicating the successful formation of Fe_3O_4@PB composites.

Transmission electronic microscopy (TEM) was used to characterize the Fe_3O_4@PB NPs (Figure 2c,d). Different from Fe_3O_4 NPs with diameters around 15−20 nm, the as-synthesized Fe_3O_4@PB NPs showed an obvious core−shell structure. The thickness of the nanoshells and diameters of the nanocores were 3−5 and 15−20 nm, respectively. The result further demonstrated the successful fabrication of the Fe_3O_4@PB NPs. During the consecutive addition of $[Fe(CN)_6]^{4-}$ and Fe^{3+} to Fe_3O_4 NPs, PB nanoshells were grown around Fe_3O_4 NPs surfaces with abundant Fe^{3+} under acidic condition. According to the literature,[30] the percentage of PB nanoshells accounted for about 50% of the whole core−shell NPs prepared with a similar method. The thickness of PB nanoshells could be controlled by varying the number of addition circles of $[Fe(CN)_6]^{4-}$ and Fe^{3+}. Nevertheless, one addition cycle was sufficient since further growth of PB nanoshells would reduce their magnetic properties.

Magnetic Property and *In Vitro* MRI Contrast Enhancement of Fe_3O_4@PB NPs. Magnetic properties of the obtained Fe_3O_4@PB NPs were studied primarily. Aqueous dispersions of the NPs were placed near a magnet to investigate their potential for magnetic targeting as shown in Figure 3a. Both Fe_3O_4 NPs and the Fe_3O_4@PB NPs showed rapid movement toward the magnet within 10 min, while PB NPs exhibited no apparent change, suggesting great potential of the Fe_3O_4@PB NPs for magnetic targeting.

Field-dependent magnetization measurement was further used to study their magnetic properties. Figure 3b shows magnetization curves of the NPs at room temperature. Although the Fe_3O_4@PB NPs (48.3 emu·g^{-1}) showed lower saturation magnetization than that of Fe_3O_4 NPs, no hysteresis or remnant magnetization was observed. The result demonstrated superparamagnetism of the Fe_3O_4@PB NPs due to the existence of Fe_3O_4 nanocores. Because of the superparamagnetism, Fe_3O_4 NPs had been approved by U.S. FDA for clinical MRI applications.[22,28,31,32]

To investigate the potential of the Fe_3O_4@PB NPs as a contrast agent for MRI, *in vitro* T_2-weighted MRI was performed on a 3.0 T MR scanner as shown in Figure 3c. Using deionized water as the control, an increasingly darkening effect in the T_2-weighted magnetic resonance images was observed with the increase of iron concentration in the NPs. The result implied the typical iron concentration-dependent T_2-weighted MRI contrast enhancement effect.[33,34] Figure 3d shows T_2 relaxation rate ($1/T_2$) as a function of iron concentration in the Fe_3O_4@PB NPs. The T_2 relaxation time decreased as the iron concentration increased with a linear relationship between the relaxation rate and iron concentration in the concentration range from 0.21 to 1.26 mM. The weighted transverse relaxivity value (r_2) was measured to be 58.9 mM^{-1}·s^{-1}, which was in good agreement with most reported values.[35]

Photothermal Effect of Fe_3O_4@PB NPs. PB NPs had been explored as the new generation of NIR-driven photothermal agent for photothermal therapy of cancers.[7] As formerly shown in Figure 2b, the Fe_3O_4@PB NPs exhibited a

dx.doi.org/10.1021/bc500279w | *Bioconjugate Chem.* 2014, 25, 1655−1663

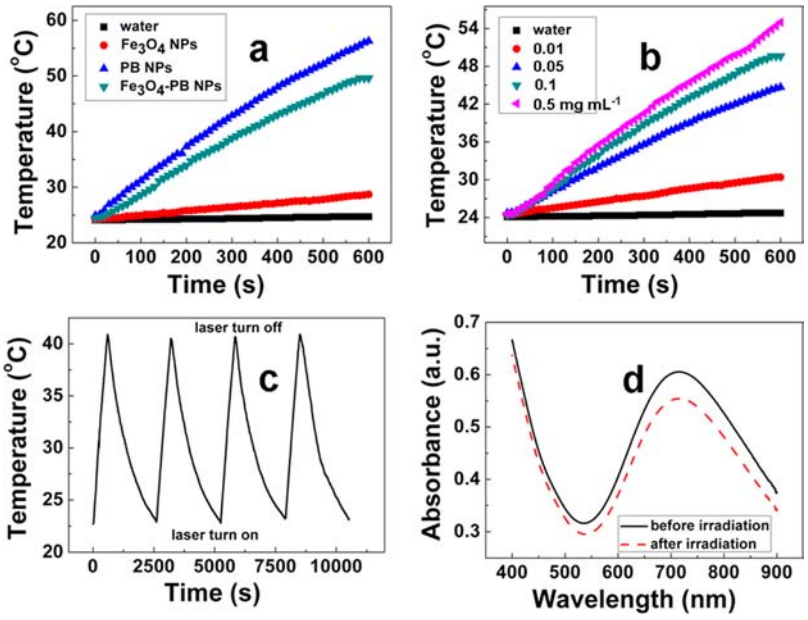

Figure 4. (a) Temperature change of different nanoparticle dispersions (0.5 mg·mL^{-1}) during laser irradiation procedure. (b) Temperature change of Fe_3O_4@PB NPs with different concentrations during NIR laser irradiation. (c) Temperature variations of Fe_3O_4@PB NPs dispersions (0.05 mg·mL^{-1}) during 4 irradiation cycles. (d) UV−vis absorption spectra of Fe_3O_4@PB NPs dispersions before and after 4 irradiation cycles. The irradiation was carried out with a NIR laser with the wavelength of 808 nm at 1.5 W·cm^{-2}.

strong absorption peak in the NIR region at about 700 nm, indicating the possibility of the core−shell NPs for photothermal conversion in the NIR region.

To study the photothermal effect, aqueous dispersions of the NPs were exposed to a laser with the wavelength of 808 nm and the output power of 2.0 W. Figure 4a shows the temperature elevation of different nanoparticle dispersions during the irradiation process. Both the Fe_3O_4@PB NPs and PB NPs exhibited dramatically increased temperature during irradiation while no significant temperature change was observed in the case of water and Fe_3O_4 NPs. With the increase of the nanoparticle concentration, the temperature elevation rate increased obviously as shown in Figure 4b. The Fe_3O_4@PB NPs with low concentration of 0.01 mg·mL^{-1} can lead to a temperature elevation of 7.0 °C from the initial value. Irradiation of the NPs of only 0.05 mg·mL^{-1} for 10 min was sufficient to reach the critical temperature (43 °C)[1] needed for killing of cancer cells.

To investigate the photothermal stability of the Fe_3O_4@PB NPs, the nanoparticle dispersions were continuously re-exposed to a laser with the wavelength of 808 nm. Figure 4c shows the temperature changes of the dispersions during 4 irradiation cycles. Significantly, the Fe_3O_4@PB NPs exhibited stable temperature elevation during 4 cycles, implying good photothermal stability of the Fe_3O_4@PB NPs attributed to the high structural stability of the PB.[7] In addition, only minor change in UV−vis absorption spectra of the nanoparticle dispersions was observed before and after 4 irradiation cycles as shown in Figure 4d, further confirming good photothermal stability of the Fe_3O_4@PB NPs. The colorimetric observation method was also used to verify the photothermal stability as shown in the Supporting Information (Figure S1).

Magnetically Targeted Photothermal Cytotoxicity *In Vitro*. Biocompatibility of the Fe_3O_4@PB NPs to normal human umbilical vein endothelial cells (HUVEC) was studied with the conventional MTT assay prior to their application for PTT treatment of cancer cells. The viabilities of HUVEC cells after the incubation with various concentrations of the Fe_3O_4@PB NPs for 24 h were studied as shown in the Supporting Information (Figure S2). There was no apparent change in cell viability in the concentration range below 0.32 mg·mL^{-1}, indicating reliable biocompatibility of the Fe_3O_4@PB NPs.

To evaluate the magnetically targeted tumor photohyperthermic effect of the Fe_3O_4@PB NPs, HeLa cells incubated with the NPs in 6-well plates were irradiated with a laser (808 nm, 1.5 w·cm^{-2}, 10 min) with and without the magnetic targeting of the NPs to the cell-growing plate bottom by using an external magnetic field. Calcein AM was then used to stain HeLa cells for assessment of cell viability as shown in Figure 5. In the presence of either the NPs or laser irradiation alone (a−c), HeLa cells showed entire vivid green fluorescence, indicating the survival of HeLa cells. Similarly, the presence of both the NPs and external magnetic field could not lead to cell death in the absence of laser irradiation (d). Also, no cell death was observed in the presence of a low concentration of the NPs (0.025 mg·mL^{-1}) and laser irradiation in the absence of external magnetic field (e), since the temperature elevation was not enough to kill cancer cells. On the contrary, with the aid of external magnetic field (f), a dark region indicating cell death was observed in the presence of the same low concentration of the NPs and laser irradiation. The dark region matched well with the irradiation site of the laser on the well. These results suggested that the usage of magnetic targeting could greatly improve the photothermal ablation effect of the NPs to cancer cells.

To further confirm the magnetic targeting effect of the Fe_3O_4@PB NPs to cancer cells, cellular micromorphology of the above HeLa cells treated with and without the usage of external magnetic field was studied. Figure 6a−c shows TEM images of thin sections of HeLa cells after incubation for 24 h with the Fe_3O_4@PB NPs (0.05 mg·mL^{-1}). The control HeLa cells (a) without the incubation with the NPs exhibited a typical

dx.doi.org/10.1021/bc500279w | *Bioconjugate Chem.* 2014, 25, 1655−1663

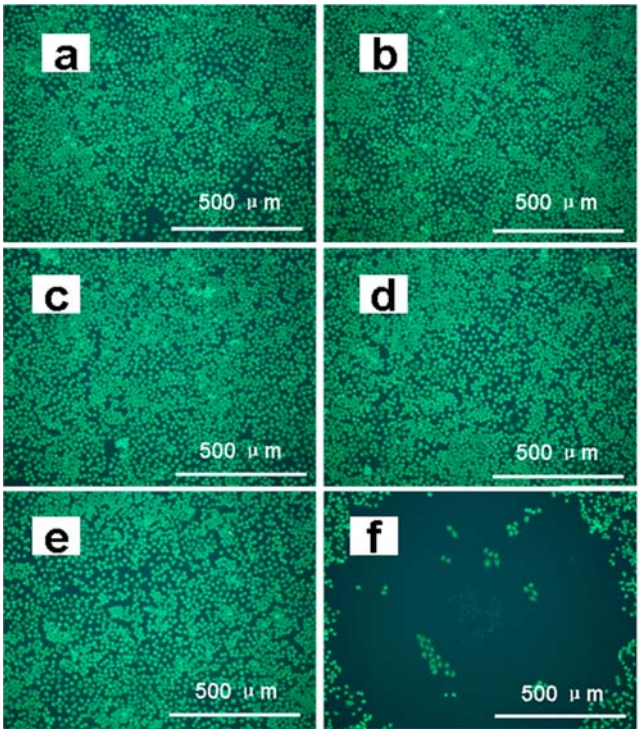

Figure 5. Fluorescence microscopic images of HeLa cells with different treatments of the Fe_3O_4@PB NPs agent (0.025 mg·mL^{-1}) after calcein AM staining: (a) no agent, no irradiation; (b) no agent, irradiation; (c) agent, no irradiation; (d) agent, magnetic targeting, no irradiation; (e) agent, irradiation; (f) agent, magnetic targeting, laser irradiation. The irradiation was carried out with a NIR laser with the wavelength of 808 nm at 1.5 W·cm^{-2} for 10 min.

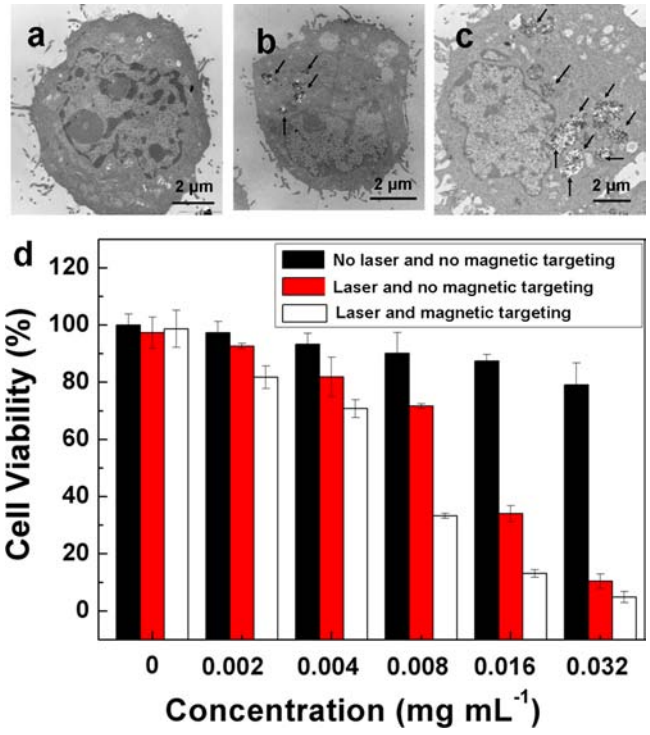

Figure 6. TEM images of thin sections of HeLa cells after the incubation for 24 h with (a) 0 mg·mL^{-1} of the Fe_3O_4@PB NPs, (b) 0.05 mg·mL^{-1} of the Fe_3O_4@PB NPs without and (c) with the usage of magnetic targeting; (d) viabilities of HeLa cells treated with different concentrations of the Fe_3O_4@PB NPs with and without the laser irradiation (808 nm, 1.5 W·cm^{-2}, 10 min) and the usage of magnetic targeting.

cellular micromorphology with obvious cellular microstructures. Yet, after incubation with the core−shell NPs (b), a small amount of NPs were clearly observed in the cells. These NPs appeared to be localized in vesicles within the cytoplasm of the cells. Previous studies reported that inorganic NPs with similar diameters such as PB NPs[18] and gold NPs[18] could be readily taken up by cells via endocytosis. Interestingly, a greatly increased amount of the NPs were observed in vesicles within cytoplasm of the HeLa cells by applying an external magnetic field (c). This demonstrated that the utilization of an external magnetic field improved intracellular internalization of the NPs, hence leading to an enhanced photohyperthermic effect to cancer cells.

The magnetically targeted photothermal cytotoxicity of the Fe_3O_4@PB NPs to HeLa cells was further monitored with the MTT assay as shown in Figure 6d. There was no apparent change in cell viability in the presence of the Fe_3O_4@PB NPs in the concentration range from 0 to 0.032 mg·mL^{-1} without applying both external magnetic field and laser irradiation. In contrast, high photothermal cytotoxicity was seen at various nanoparticle concentrations in the presence of external magnetic field. After treatment with 0.016 mg·mL^{-1} Fe_3O_4@PB NPs and laser irradiation, the employment of external magnetic field resulted in less than 20% of cell viability. Statistically significant difference induced by applying the magnetic field could be observed at rather low concentration of Fe_3O_4@PB NPs (0.002 mg·mL^{-1}). These results further demonstrated that even low concentrations of Fe_3O_4@PB NPs could effectively cause the death of cancer cells through their magnetically targeted photothermal effect.

***In Vivo* MRI Contrast Enhancement.** *In vivo* T_2-weighted MRI using the Fe_3O_4@PB NPs was carried out with the U87MG tumor-bearing nude mouse model. The nanoparticle aqueous dispersions (0.1 mL, 2.0 mg·ml^{-1}) were intratumorally injected into the tumor-bearing nude mice. The nude mice were then scanned with a 3.0 T whole-body MR scanner to study the *in vivo* MRI contrast enhancement effect as shown in Figure 7.

Dramatically increased darkening effect in the magnetic resonance images was observed around the tumor site after the injection of the Fe_3O_4@PB NPs (b). The result demonstrated that the Fe_3O_4@PB NPs exhibited considerable contrast enhancement effect for *in vivo* T_2-weighted MRI. Due to the ease of identification of tumor locations and assessment of therapeutic efficacy, MRI had been widely applied for the guidance of various therapies, especially photothermal therapy.[36−38] Therefore, the Fe_3O_4@PB NPs could serve as a theranostic nanomedicine capable of noninvasive MRI diagnosis and MRI-guided photothermal therapy.

***In Vivo* Photothermal Ablation of Tumors with Fe_3O_4@PB NPs.** To evaluate the *in vivo* photothermal therapeutic effect of the Fe_3O_4@PB NPs, U87MG tumor-bearing nude mice were intratumorally injected with aqueous suspensions of the NPs (0.1 mL, 1.0 mg·ml^{-1}), which were then irradiated with a NIR laser with the wavelength of 808 nm and the output power of 2.0 W for 10 min. Various control groups with different treatments were carried out for comparison.

The temperature variation in tumor tissues was primarily monitored during the irradiation as shown in Figure 8a. There

dx.doi.org/10.1021/bc500279w | *Bioconjugate Chem.* 2014, 25, 1655−1663

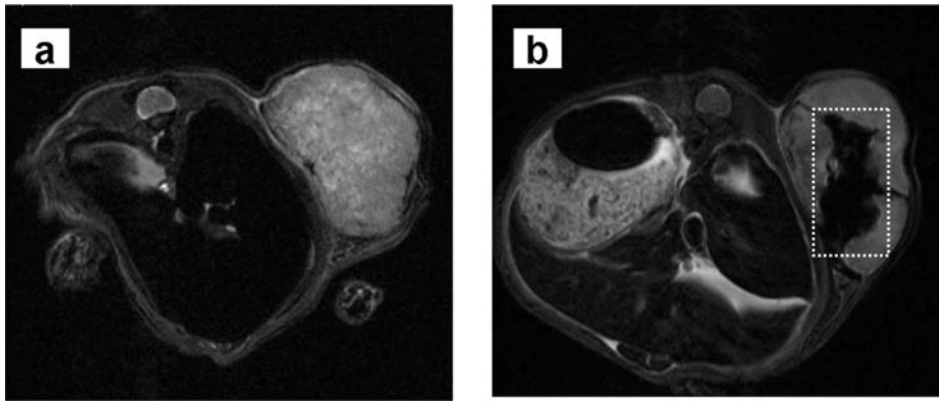

Figure 7. *In vivo* T_2-weighted MR images of U87MG tumor-bearing nude mouse (a) before and (b) after the intratumoral injection of the Fe_3O_4@PB NPs dispersions (0.1 mL, 2.0 mg·mL^{-1}).

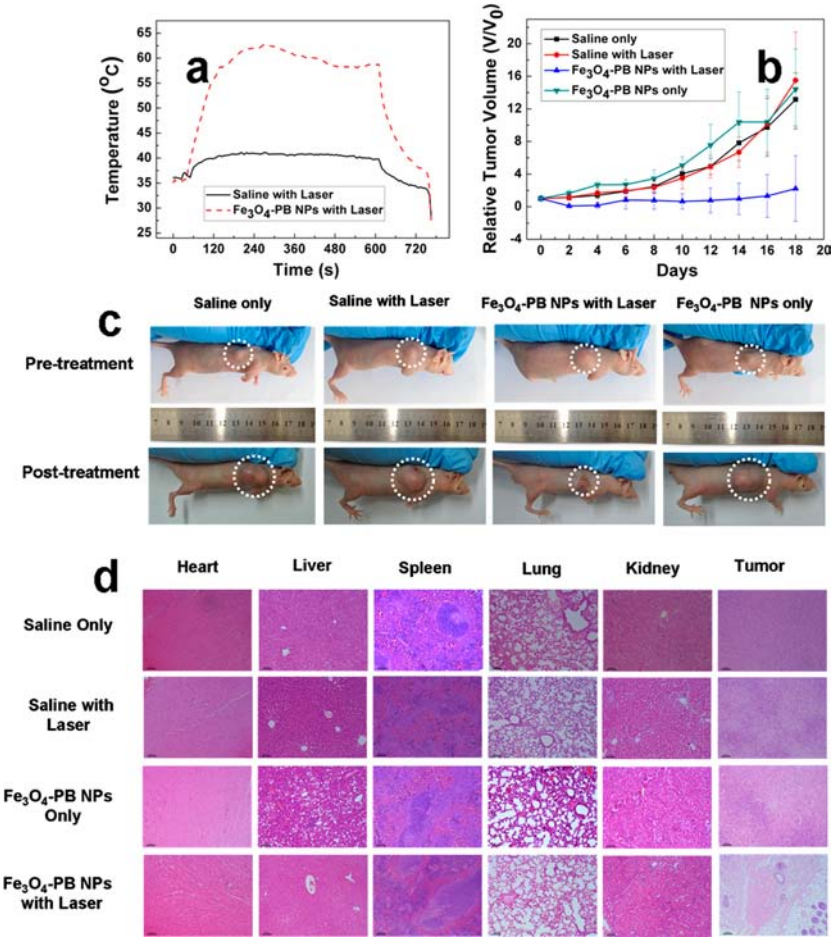

Figure 8. (a) *In vivo* temperature variation of the tumor tissues with the injection of saline and the Fe_3O_4@PB NPs (0.1 mL, 1.0 mg·mL^{-1}) upon irradiation with a NIR laser (808 nm, 1.5 W·cm^{-2}) for 10 min. (b) Tumor growth curves of various groups of the mice with different treatments. The tumor volume was normalized to the initial size. (c) Photographs of various groups of mice before and after different treatments. (d) H&E stained images of heart, liver, spleen, lung, kidney, and tumor collected from mice of various groups with different treatments after 18 days.

was only a slight temperature elevation for the control group with the injection of saline during the irradiation for 10 min while a dramatic temperature elevation was observed with the injection of the Fe_3O_4@PB NPs (0.1 mL, 1.0 mg·mL^{-1}). The temperature was elevated to more than 60 °C from the body temperature, which could ablate cancer cells efficiently through the hyperthermic effect.

The tumor size was tested every 2 days after the treatment to investigate the *in vivo* photothermal therapeutic effect of the Fe_3O_4@PB NPs. Figure 8b,c shows the tumor growth status of various mice groups with different treatments. The control groups with the injection of saline and the Fe_3O_4@PB NPs without the laser irradiation showed obviously rapid tumor growth within 18 days. A high relative volume (V/V_0 = 15.6) of the tumor size was observed after 18 days. In contrast, mice

dx.doi.org/10.1021/bc500279w | *Bioconjugate Chem.* 2014, 25, 1655−1663

treated with both the Fe_3O_4@PB NPs and laser irradiation exhibited very low tumor growth rate with an average relative tumor volume of 2.0 after 18 days, implying a tumor inhibition rate of 87.2%. The result indicated that the Fe_3O_4@PB NPs exhibited remarkably high photothermal therapeutic efficacy *in vivo*. In addition, neither mice death nor significant body weight variation of the mice was observed in all groups during the experimental period (Supporting Information, Figure S3), implying reliable biosafety of the NPs *in vivo*.

Mice were sacrificed for necropsy after 18 days to further study the toxicity and photothermal therapeutic effect of the Fe_3O_4@PB NPs *in vivo*. Major organs of the mice with different treatments were collected for histological examination as shown in Figure 8d. No apparent organ damage or abnormality in heart, liver, spleen, lung, and kidney was observed for all mice from the H&E stained organ slices, demonstrating good biocompatibility of the Fe_3O_4@PB NPs *in vivo*. Significantly, mice treated with both the Fe_3O_4@PB NPs and laser irradiation showed obvious organ damage in tumor tissues in comparison with the control groups, further revealing the effective hyperthermic effect of the Fe_3O_4@PB NPs to tumors.

■ CONCLUSIONS

Theranostic Fe_3O_4@PB core−shell NPs were constructed by growing PB nanoshells of 3−6 nm around superparamagnetic Fe_3O_4 nanocores through a shell-growing procedure. The obtained Fe_3O_4@PB NPs were found to show promising magnetic targeting capability, *in vivo* MRI contrast enhancement and photothermal effect for tumor ablation, thus permitting highly efficient MRI-guided targeted photothermal therapy of cancers. Most importantly, both PB and Fe_3O_4 nanoparticles are typical U.S. FDA-approved drugs, so the composite Fe_3O_4@PB NPs would have great potential as a new generation of theranostic nanomedicine for clinical applications.

■ MATERIALS AND METHODS

Materials. 3-(4,5-Dimethylthiazol-2-yl)-2,5-diphenyltetrazolium bromide (MTT) and calcein acetoxymethyl ester (Calcein AM) were obtained from Sigma. Unless otherwise stated, reagents were of analytical reagent grade. Aqueous solutions were prepared with deionized water (18.2 MΩ cm) collected from a Milli-Q system.

Synthesis of Fe_3O_4@PB NPs. The Fe_3O_4@PB NPs were synthesized by an improved shell-growing procedure according to the literature.[19,30] Briefly, 10 mL Fe_3O_4 NPs aqueous dispersion was added dropwise into 20 mL aqueous $K_4[Fe(CN)_6]$ solution (2.0 mM, pH = 3.0) under vigorous mechanical stirring at room temperature. The color of the Fe_3O_4 NP aqueous dispersion gradually changed to light green during the addition process. Then, 20 mL aqueous $FeCl_3$ solution (2.0 mM, pH = 3.0) was added dropwise into the above mixed solution. The obtained Fe_3O_4@PB NPs were separated from the aqueous solution and washed three times with deionized water using an external magnetic field. The obtained composite NPs were finally redispersed in deionized water to form the aqueous dispersion of the Fe_3O_4@PB NPs.

***In Vitro* and *In Vivo* Magnetic Resonance Imaging.** The magnetic resonance imaging experiments were performed with a Philips 3.0 T whole-body magnetic resonance imaging scanner (PHILIPS-14B464A). Nude mice were obtained from Peking University Third Hospital (PUTH) and used under protocols approved by the Animal Center of PUTH. For *in vitro* magnetic resonance imaging, the microscopic transverse relaxation time (T_2) was measured with various concentrations of the Fe_3O_4@PB NPs by applying the spin−echo (SE) sequences at room temperature with the repetition time (TR) of 787.0 ms, the echo time (TE) of 90.0 ms and the section thickness of 2.50 mm. The relaxivity value (r_2, $mM^{-1}\cdot s^{-1}$) was calculated using T_2 measurements of different concentrations of the NPs in deionized water. The *in vivo* magnetic resonance imaging experiment was carried out with the U87MG tumor-bearing nude mouse model. 2×10^6 U87MG cancer cells suspended in cell medium were injected on the shoulder of each nude mouse to obtain U87MG tumor-bearing nude mouse model. 0.1 mL aqueous dispersions of the Fe_3O_4@PB NPs (2.0 $mg\cdot mL^{-1}$) were injected into the tumor sites of the nude mouse after 1 week for *in vivo* magnetic resonance imaging on a Philips 3.0 T whole-body magnetic resonance imaging scanner (PHILIPS-14B464A).

***In Vivo* Photothermal Therapy.** The *in vivo* photothermal therapeutic experiment was carried out with the U87MG tumor-bearing nude mouse model obtained from Peking University Third Hospital (PUTH). 0.1 mL saline or aqueous suspensions of the Fe_3O_4@PB NPs (1.0 $mg\cdot mL^{-1}$) were injected into the tumor sites. Four groups of mice, including that treated with the injection of saline only, injection of saline with laser irradiation, injection of Fe_3O_4@PB NPs only, and injection of Fe_3O_4@PB NPs with laser irradiation, with seven mice per group were used. After the intratumoral injection of saline or aqueous suspensions of the Fe_3O_4@PB NPs, the tumors on the mice were irradiated with an 808 nm laser (T808D2W, Xi'an Minghui Optoelectronic Technology Co., China) at 1.5 $W\cdot cm^{-2}$ for 10 min. A digital thermometer with its detecting needle inserted into the tumor sites was used to monitor the temperature variation during the laser irradiation. The tumor size was then measured every 2 days with a caliper to calculate the tumor size according to the traditional method. Mice with tumor sizes exceeding 1000 mm^3 were euthanatized according to the animal protocol.

■ ASSOCIATED CONTENT

Ⓢ Supporting Information

Detailed experimental procedures, colorimetric study on photothermal stability, biocompatibility of the core−shell magnetic PB NPs, and variation of body weight of the mice after the photothermal treatment. This material is available free of charge via the Internet at http://pubs.acs.org.

■ AUTHOR INFORMATION

Corresponding Author

*Tel.: +86-10-62767580; fax: +86-10-62767580. E-mail address: zhifei.dai@pku.edu.cn. Homepage: http://bme.pku.edu.cn/~daizhifei.

Author Contributions

The work was carried out through contributions of all authors. All authors have given the approval to the final version of the manuscript.

Notes

The authors declare no competing financial interest.

■ ACKNOWLEDGMENTS

This work was financially supported by the National Natural Science Foundation for Distinguished Young Scholars (no. 81225011), the State Key Program of National Natural Science

of China (no. 81230036), and the National Natural Science Foundation of China (no. 81371580 and 21273014).

REFERENCES

(1) Ke, H. T., Wang, J. R., Dai, Z. F., Jin, Y. S., Qu, E. Z., Xing, Z. W., Guo, C. X., Yue, X. L., and Liu, J. B. (2011) Gold-nanoshelled microcapsules: a theranostic agent for ultrasound contrast imaging and photothermal therapy. *Angew. Chem., Int. Ed. 50*, 3017−3021.

(2) Bhojani, M. S., Van Dort, M., Rehemtulla, A., and Ross, B. D. (2010) Targeted imaging and therapy of brain cancer using theranostic nanoparticles. *Mol. Pharmaceutics 7*, 1921−1929.

(3) Choi, K. Y., Jeon, E. J., Yoon, H. Y., Lee, B. S., Na, J. H., Min, K. H., Kim, S. Y., Myung, S. J., Lee, S., Chen, X., Kwon, I. C., Choi, K., Jeong, S. Y., Kim, K., and Park, J. H. (2012) Theranostic nanoparticles based on PEGylated hyaluronic acid for the diagnosis, therapy and monitoring of colon cancer. *Biomaterials 33*, 6186−6193.

(4) Guo, C. X., Jin, Y. S., and Dai, Z. F. (2014) Multifunctional ultrasound contrast agents for imaging guided photothermal therapy. *Bioconjugate Chem. 25*, 840−854.

(5) Huang, X. H., El-Sayed, I. H., Qian, W., and El-Sayed, M. A. (2006) Cancer cell imaging and photothermal therapy in the near-infrared region by using gold nanorods. *J. Am. Chem. Soc. 128*, 2115−2120.

(6) Jing, L. J., Liang, X. L., Li, X. D., Lin, L., Yang, Y. B., Yue, X. L., and Dai, Z. F. (2014) Mn-porphyrin conjugated Au nanoshells encapsulating doxorubicin for potential magnetic resonance imaging and light triggered synergistic therapy of cancer. *Theranostics 4*, 858−871.

(7) Fu, G. L., Liu, W., Feng, S. S., and Yue, X. L. (2012) Prussian blue nanoparticles operate as a new generation of photothermal ablation agents for cancer therapy. *Chem. Commun. 48*, 11567−11569.

(8) Jing, L., Liang, X., Deng, Z., Feng, S., Li, X., Huang, M., Li, C., and Dai, Z. (2014) Prussian blue coated gold nanoparticles for simultaneous photoacoustic/CT bimodal imaging and photothermal ablation of cancer. *Biomaterials 35*, 5814−5821.

(9) Hoffman, H. A., Chakrabarti, L., Dumont, M. F., Sandler, A. D., and Fernandes, R. (2014) Prussian blue nanoparticles for laser-induced photothermal therapy of tumors. *RSC Adv. 4*, 29729−29734.

(10) Coughlin, A. J., Ananta, J. S., Deng, N., Larina, I. V., Decuzzi, P., and West, J. L. (2014) Gadolinium-conjugated gold nanoshells for multimodal diagnostic imaging and photothermal cancer therapy. *Small 10*, 556−565.

(11) Moon, H. K., Lee, S. H., and Choi, H. C. (2009) In vivo near-infrared mediated tumor destruction by photothermal effect of carbon nanotubes. *ACS Nano 3*, 3707−3713.

(12) Neves, L. F., Krais, J. J., Van Rite, B. D., Ramesh, R., Resasco, D. E., and Harrison, R. G. (2013) Targeting single-walled carbon nanotubes for the treatment of breast cancer using photothermal therapy. *Nanotechnology 24*, 375104.

(13) Hashida, Y., Tanaka, H., Zhou, S., Kawakami, S., Yamashita, F., Murakami, T., Umeyama, T., Imahori, H., and Hashida, M. (2014) Photothermal ablation of tumor cells using a single-walled carbon nanotube-peptide composite. *J. Controlled Release 173*, 59−66.

(14) Lin, J., Wang, S., Huang, P., Wang, Z., Chen, S., Niu, G., Li, W., He, J., Cui, D., Lu, G., Chen, X., and Nie, Z. (2013) Photosensitizer-loaded gold vesicles with strong plasmonic coupling effect for imaging-guided photothermal/photodynamic therapy. *ACS Nano 7*, 5320−5329.

(15) Jang, B., Park, J. Y., Tung, C. H., Kim, I. H., and Choi, Y. (2011) Gold nanorod-photosensitizer complex for near-infrared fluorescence imaging and photodynamic/photothermal therapy in vivo. *ACS Nano 5*, 1086−1094.

(16) Nam, J., Won, N., Jin, H., Chung, H., and Kim, S. (2009) pH-Induced aggregation of gold nanoparticles for photothermal cancer therapy. *J. Am. Chem. Soc. 131*, 13639−13645.

(17) Liu, H., Chen, D., Li, L., Liu, T., Tan, L., Wu, X., and Tang, F. (2011) Multifunctional gold nanoshells on silica nanorattles: a platform for the combination of photothermal therapy and chemotherapy with low systemic toxicity. *Angew. Chem., Int. Ed. 50*, 891−895.

(18) Shokouhimehr, M., Soehnlen, E. S., Hao, J. H., Griswold, M., Flask, C., Fan, X. D., Basilion, J. P., Basu, S., and Huang, S. D. (2010) Dual purpose Prussian blue nanoparticles for cellular imaging and drug delivery: a new generation of T-1-weighted MRI contrast and small molecule delivery agents. *J. Mater. Chem. 20*, 5251−5259.

(19) Zhang, X. Q., Gong, S. W., Zhang, Y., Yang, T., Wang, C. Y., and Gu, N. (2010) Prussian blue modified iron oxide magnetic nanoparticles and their high peroxidase-like activity. *J. Mater. Chem. 20*, 5110−5116.

(20) Dumont, M. F., Hoffman, H. A., Yoon, P. R. S., Conklin, L. S., Saha, S. R., Paglione, J. P., Sze, R. W., and Fernandes, R. (2014) Biofunctionalized gadolinium-containing prussian blue nanoparticles as multimodal molecular imaging agents. *Bioconjugate Chem. 25*, 129−137.

(21) Santra, S., Kaittanis, C., Grimm, J., and Perez, J. M. (2009) Drug/dye-loaded, multifunctional iron oxide nanoparticles for combined targeted cancer therapy and dual optical/magnetic resonance imaging. *Small 5*, 1862−1868.

(22) Yang, F., Li, Y., Chen, Z., Zhang, Y., Wu, J., and Gu, N. (2009) Superparamagnetic iron oxide nanoparticle-embedded encapsulated microbubbles as dual contrast agents of magnetic resonance and ultrasound imaging. *Biomaterials 30*, 3882−3890.

(23) Hultman, K. L., Raffo, A. J., Grzenda, A. L., Harris, P. E., Brown, T. R., and O'Brien, S. (2008) Magnetic resonance imaging of major histocompatibility class II expression in the renal medulla using immunotargeted superparamagnetic iron oxide nanoparticles. *ACS Nano 2*, 477−484.

(24) Ma, X. X., Tao, H. Q., Yang, K., Feng, L. Z., Cheng, L., Shi, X. Z., Li, Y. G., Guo, L., and Liu, Z. (2012) A functionalized graphene oxide-iron oxide nanocomposite for magnetically targeted drug delivery, photothermal therapy, and magnetic resonance imaging. *Nano. Res. 5*, 199−212.

(25) Zhang, J., Shin, M. C., and Yang, V. C. (2014) Magnetic targeting of novel heparinized iron oxide nanoparticles evaluated in a 9L-glioma mouse model. *Pharm. Res. 31*, 579−592.

(26) Zhou, J., Zhang, J., David, A. E., and Yang, V. C. (2013) Magnetic tumor targeting of beta-glucosidase immobilized iron oxide nanoparticles. *Nanotechnology 24*, 375102.

(27) Wang, Y. X. (2011) Superparamagnetic iron oxide based MRI contrast agents: Current status of clinical application. *Quant. Imaging Med. Surg. 1*, 35−40.

(28) http://www.drugs.com/pro/feridex.html.

(29) http://www.fda.gov/drugs/emergencypreparedness/bioterrorismanddrugpreparedness/ucm130334.htm.

(30) Thammawong, C., Opaprakasit, P., Tangboriboonrat, P., and Sreearunothai, P. (2013) Prussian blue-coated magnetic nanoparticles for removal of cesium from contaminated environment. *J. Nanopart. Res. 15*, 1689.

(31) Zhao, Z. H., Zhou, Z. J., Bao, J. F., Wang, Z. Y., Hu, J., Chi, X. Q., Ni, K. Y., Wang, R. F., Chen, X. Y., Chen, Z., and Gao, J. H. (2013) Octapod iron oxide nanoparticles as high-performance T-2 contrast agents for magnetic resonance imaging. *Nat. Commun. 4*, 2266.

(32) Poselt, E., Kloust, H., Tromsdorf, U., Janschel, M., Hahn, C., Masslo, C., and Weller, H. (2012) Relaxivity optimization of a PEGylated iron-oxide-based negative magnetic resonance contrast agent for T-2-weighted spin-echo imaging. *ACS Nano 6*, 1619−1624.

(33) Su, H. Y., Liu, Y. H., Wang, D., Wu, C. Q., Xia, C. C., Gong, Q. Y., Song, B., and Ai, H. (2013) Amphiphilic starlike dextran wrapped superparamagnetic iron oxide nanoparticle clsuters as effective magnetic resonance imaging probes. *Biomaterials 34*, 1193−1203.

(34) Ahmad, T., Bae, H., Rhee, I., Chang, Y., Jin, S. U., and Hong, S. (2012) Gold-coated iron oxide nanoparticles as a T-2 contrast agent in magnetic resonance imaging. *J. Nanosci. Nanotechnol. 12*, 5132−5137.

(35) Ma, Y., Liang, X. L., Tong, S., Bao, G., Ren, Q. S., and Dai, Z. F. (2013) Gold nanoshell nanomicelles for potential magnetic resonance imaging, light-triggered drug release, and photothermal therapy. *Adv. Funct. Mater. 23*, 815−822.

(36) Yang, H. W., Liu, H. L., Li, M. L., Hsi, I. W., Fan, C. T., Huang, C. Y., Lu, Y. J., Hua, M. Y., Chou, H. Y., Liaw, J. W., Ma, C. C., and

Wei, K. C. (2013) Magnetic gold-nanorod/PNIPAAmMA nanoparticles for dual magnetic resonance and photoacoustic imaging and targeted photothermal therapy. *Biomaterials 34*, 5651−5660.
(37) Chen, Y. C., Gnyawali, S. C., Wu, F., Liu, H., Tesiram, Y. A., Abbott, A., Towner, R. A., and Chen, W. R. (2008) Magnetic resonance imaging guidance for laser photothermal therapy. *J. Biomed. Opt. 13*, 044033.
(38) Wang, D. W., Zhu, X. M., Lee, S. F., Chan, H. M., Li, H. W., Kong, S. K., Yu, J. C., Cheng, C. H. K., Wang, Y. X. J., and Leung, K. C. F. (2013) Folate-conjugated Fe3O4@SiO2@gold nanorods@mesoporous SiO2 hybrid nanomaterial: a theranostic agent for magnetic resonance imaging and photothermal therapy. *J. Mater. Chem. B 1*, 2934−2942.